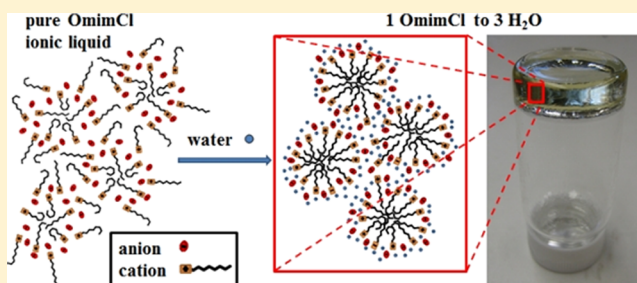# Orientational Dynamics in a Lyotropic Room Temperature Ionic Liquid

Adam L. Sturlaugson, Aaron Y. Arima, Heather E. Bailey, and Michael D. Fayer*

Department of Chemistry, Stanford University, Stanford, California 94305, United States

ABSTRACT: In a previous study of room temperature ionic liquid/water mixtures, the first clearly observed biexponential decays in optical heterodyne-detected optical Kerr effect (OHD-OKE) experiments on a liquid were reported, (Sturlaugson, A. L.; Fruchey, K. S.; Fayer, M. D. *J. Phys. Chem. B* **2012**, *116*, 1777), and it was suggested that the biexponential behavior is indicative of the approach to gelation. Here, new OHD-OKE experiments on mixtures of the room temperature ionic liquid 1-methyl-3-octylimidazolium chloride (OmimCl) with water are presented. The OmimCl/water system is shown to gel over the water mole fraction range of 0.69−0.81. In the OHD-OKE decays, the biexponential behavior becomes more distinct as the gelling concentration range is approached from either high or low water concentrations. The biexponential decays are analyzed in terms of the wobbling-in-a-cone model, and the resulting diffusion constants and "relative" order parameters and cone angles are reported. Comparison of the OmimCl/water data with the previously reported room temperature ionic liquid/water OHD-OKE decays supports the previous hypothesis that the biexponential dynamics are due to the approach to the liquid−gel transition and suggests that the order of the concentration-dependent phase transition can be tuned by the choice of anion.
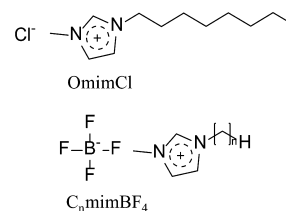
I. INTRODUCTION

Room temperature ionic liquids (or RTILs, salts with a melting point below 25 °C) have become a subject of intense study over the last several decades. Since the turn of the century, research in RTILs has exploded, impacting many fields of science and engineering. Currently, RTIL application research includes synthesis, batteries, solar cells, crystallization, drug delivery, and optics.[1−8]

Because the constituent ions in RTILs are highly variable,[1] their molecular properties display a diverse range of features, e.g., redox activity,[9] fluorescence,[10] and paramagnetism.[11] The mesoscopic and macroscopic properties of RTILs can also be quite complex. For example, short-chain alkylimidazolium RTILs are isotropic liquids, but those with longer chains display liquid crystalline behavior.[12,13] Many of the pure, nominally isotropic RTILs display nanoscale ordering not seen in most molecular liquids.[14−16] When additional components are added to RTILs, the macroscopic behavior can become even more diverse. Some binary mixtures of pure RTILs show gelation behavior,[17] and some can be gelled with simple small molecule "gelators" to form what is now called an ionogel.[18,19] Of considerable interest are the RTILs that undergo gelation simply by addition of water.[20−23] Members of this latter group are probably better classified as lyotropic liquid crystals, since many reports indicate formation of lamellar, cubic, hexagonal, and micellular phases as the water concentration is increased.[21,22,24] The fact that mixing water with some RTILs (i.e., mixing two liquids) can lead to stable gel formation may be unique to this class of liquids. Of those RTILs that show this hydrogel/ionogel behavior, the RTIL 1-methyl-3-octylimidazolium chloride (OmimCl, Figure 1) is of particular interest. The gel has a melting temperature just above room temperature,[22] and OmimCl, to the best of our knowledge, is the smallest hydrogelator known.

Figure 1. The structures of the 1-methyl-3-octylimidazolium chloride and 1-alkyl-3-methylimidazolium tetrafluoroborate RTILs (OmimCl and $C_n$mimBF$_4$, respectively).

There are extensive reports of the aggregation behavior of RTILs in water, but most focus on the region of dilute RTIL in water or study RTILs that do not show gelation.[25−39] Studies of gelling systems have largely focused on the structure of the gel.[20−22,24,40−44] Dynamical measurements of gelling RTIL/water systems are limited in number and scope.[45−47] Previously, optical heterodyne-detected optical Kerr effect (OHD-OKE) experiments on a series of 1-alkyl-3-methylimidazolium tetrafluoroborate RTILs ($C_n$mimBF$_4$, Figure 1) mixed

Table 1. OmimCl/Water Mixture DSE and Wobbling-in-a-Cone Parameters

sample (mole ratio OmimCl:water)	mole fraction water	viscosity[a] (cP)	τ_c^b (ns)	τ_m (ns)	$1/6D_c^b$ (ns)	$6D_c\tau_m$	"relative" order parameter S^2	"relative" cone angle θ^d (deg)
21:1 (pure)	0.0455	14500		320^b				
2.2:1	0.310	2160	53	270^c	77	4	0.37^c	45
1:1	0.508	997	14.7	200^b	17	12	0.33^b	47
1:2	0.666	453	4.1	80^b	4.3	18	0.29^b	50
1:4.5	0.818	192	1.09	76^b	2.3	33	0.62^b	32
1:6	0.858	119	0.68	28^b	1.04	27	0.49^b	38
1:15	0.938	17.6	0.27	2.4^c	0.22	11	0.09^c	65
1:30	0.968	4.78	0.21	3.6^c	0.18	20	0.15^c	60
1:100	0.990	1.36		0.14^d				

[a]Interpolated from ref 49. [b]Error bars: ±10%. [c]Error bars: ±20%. [d]Error bars: ±5%.

with water were reported.[48] These studies demonstrated that the orientational dynamics, as probed by the OHD-OKE, anomalously slow down as water is added to the longer chain RTILs. The orientational relaxation (rotational diffusion) clearly becomes biexponential with the slow decay becoming slower even as the viscosity decreases with the addition of water. This behavior was attributed to the approach to gelation.

In $C_n$mimBF$_4$ RTILs, the long chain RTIL/water mixtures phase separate prior to gelation. In this paper, we present new OHD-OKE experiments on 1-methyl-3-octylimidazolium chloride (OmimCl) mixed with water, a system which gels over a water mole fraction range of 0.69–0.81. As with the $C_n$mimBF$_4$/water system, many OmimCl/water OHD-OKE decays are biexponential, with the samples closest to the gelling region exhibiting the most pronounced biexponential behavior. As indicated by a "relative" order parameter, the imidazolium head groups show opposite trends in the degree of restricted motion as the gelling region is approached from the two concentration ends. In the water-poor mixtures, the imidazolium motions become less restricted as the gelation boundary is approached, while, on the water-rich side, they become more restricted. Reanalysis of some of the previous $C_n$mimBF$_4$/water data in terms of the "relative" order parameter gives a trend that is the opposite of that seen in the OmimCl/water data presented here. Finally, the slow component of the OmimCl/water reorientational dynamics is slower than the Debye–Stokes–Einstein prediction, although the dramatic slowdown observed in the previous $C_n$mimBF$_4$/water studies is not seen here. The biexponential OHD-OKE dynamics reported here further support the gelation onset proposal, and a comparison of the trends in the overall cation reorientational dynamics and "relative" order parameter between the $C_n$mimBF$_4$ and OmimCl systems suggests that the order of the water-induced lyotropic phase transition can be modulated by the choice of anion.

II. EXPERIMENTAL PROCEDURES

1-Methyl-3-octylimidazolium chloride (OmimCl, 99%) was purchased from Iolitec and dried under a vacuum at ∼55 °C for at least 24 h before being transferred to a nitrogen glovebox for storage. Residual water content of the purified OmimCl was measured via Karl Fischer titration to be 3700 ppm. Samples ranging from pure OmimCl to a water mole fraction of 0.99 (mole ratio OmimCl:water = 21:1 to 1:100) were prepared by weight using HPLC grade water. Here we define water mole fraction as moles of water/(moles of ion pairs + moles of water). Mixing was facilitated by gentle heating to reduce the overall viscosity. Once homogeneous, samples were sub-

micrometer filtered into optical grade cuvettes. Viscosities of the samples were interpolated from the literature.[49] The samples in this study fell on or within the concentrations from the literature corresponding to the liquid regions, ensuring that the interpolations to obtain the viscosities were accurate near the gel phase transition. Mole fraction water and viscosity data for each sample are reported in Table 1.

Because OmimCl is known to gel at some water concentrations, the range over which gelation occurs was determined by visual inspection. Dropwise addition of water to OmimCl was measured by mass, and the mixture was gently heated, homogenized, and allowed to cool after each drop. Stable gel formation was easily determined by inversion of the sample vial (see Figure 2). The process was repeated until both the liquid-to-gel and the gel-to-liquid phase transitions were
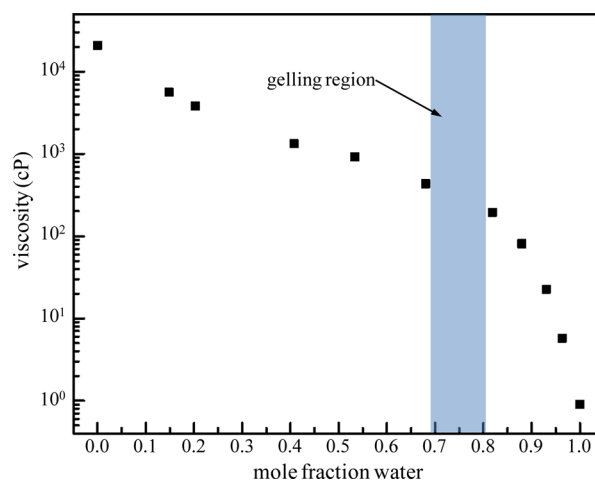

Figure 2. The figure shows a photograph of a sample vial with the OmimCl/water gel in which the vial has been inverted. The silver color is the reflection of light from the gel. The gel is stable for weeks and resists flow even when the sample vial is upside down as in the photograph.

crossed. The water-poor gel boundary occurred at a water mole fraction of 0.69 (OmimCl:water = 1:2.2) and was well-defined. The water-rich gel boundary was not quite as pronounced and occurred over the water mole fraction range 0.80–0.82 (midpoint of OmimCl:water = 1:4.4) .

The OHD-OKE is a non-resonant ultrafast spectroscopic technique in which a linearly polarized pump pulse induces a transient birefringence in an initially isotropic sample. The time decay of the birefringence is monitored via a time-delayed probe pulse linearly polarized at 45° relative to the pump. Optical heterodyne detection is achieved by making the probe polarization slightly elliptical, thereby introducing a collinear and in-phase local oscillator.[50,51] Because of the non-resonant nature of the experiment, the pulses can be chirped without interfering with the measured dynamics. For the shortest time scale measurements, the pulses were ~60 fs in duration. Pulses of longer duration were produced by increasing the chirp on the pulses and were used for the slower time scale portions of the decays. Scans taken with various pulse widths are then overlapped in software to produce the full OHD-OKE curve. The general details of the optical Kerr effect setup have been described previously,[48] but modifications for probing into the microsecond regime were made to improve the signal-to-noise. Briefly, a 5 kHz Ti:sapphire regenerative amplifier seeded by a mode-locked 86 MHz Ti:sapphire oscillator is used to generate laser pulses with widths varying from ~60 fs to 125 ps and powers up to 300 μJ per pulse. The laser pulses are beam split into pump and probe pulses, each of which is polarization phase cycled with a Pockels cell. The probe's ellipticity is modulated at 2.5 kHz. The pump polarization is modulated at 1.25 kHz, and the signal is detected at the 1.25 kHz frequency with a balanced detector and lock-in amplifier. To collect data past the 15 ns window of the long delay stage, continuous wave (CW) probing was implemented. A portion of the 532 nm CW oscillator pump laser is diffracted via an acousto-optic modulator to generate 2 μs pulses at 5 kHz. This CW probe is then crossed with the pump beam at the sample, and its transient response is recorded with a fast photomultiplier tube (Hamamatsu, R7400U) and fast digitizer (Agilent Acquiris DP110, 1 GS/s). For CW probing, the pump beam is an ~13 ns pulse coming from the free lasing output of the unseeded regenerative amplifier. CW probing data were scaled, over-lapped, and combined in software with the pulsed probing data to generate the full OHD-OKE decay curve. All OHD-OKE data were collected at 24.5 °C. Because of static birefringence, it was not possible to collect OHD-OKE data on samples in the gelled state.
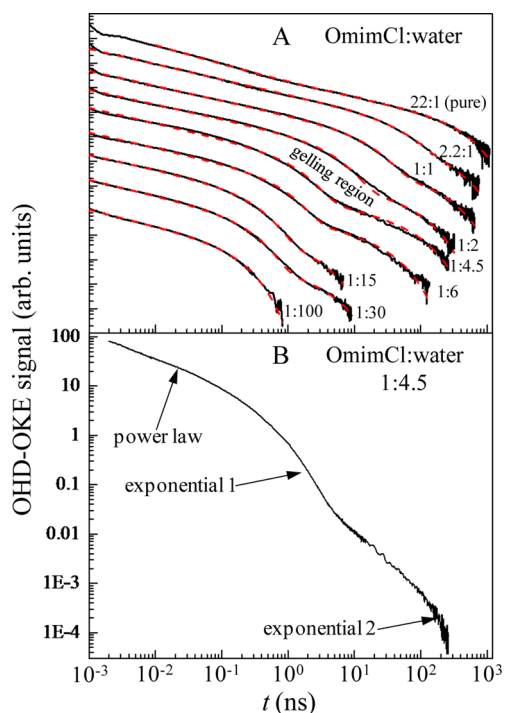
III. RESULTS AND DISCUSSION

It has been suggested that the addition of water to an RTIL screens the cation−anion attractions and "lubricates" them, reducing the overall viscosity.[52] As shown in Figure 3, the OmimCl/water mixtures appear to follow this trend (data from Gomez et al.[49]). Note the log axes. Clearly, a small amount of water quickly decreases the overall viscosity of the system. However, in this OmimCl/water system, there is a range of water concentrations over which the mixture gels (OmimCl:-water = 1:2.2 to 1:4.4, see Figure 2). This region is indicated by the blue area in Figure 3. Thus, as water is added to the system, its viscosity decreases until it abruptly gels. Further water addition induces a transition back to a liquid, and the viscosity continues to decrease as before.

Figure 3. OmimCl/water viscosity as a function of mole fraction water.[49] Note the logarithmic y-axis and the gelling region from 0.69 to 0.81.

The OHD-OKE measures the time derivative of the autocorrelation function of the polarizability anisotropy. At early times (a few ps), collision-induced effects contribute to the signal. At longer times, the polarizability autocorrelation function reduces to the second Legendre polynomial (P_2) orientational correlation function.[53−55] Because the anisotropic polarizability of water is very small compared to the cation, water does not produce an appreciable signal.[56] The chloride ion will also give negligible signal, since it is not anisotropically polarizable (due to its spherical symmetry) except at very short time when collision-induced effects are present.[57−59] Thus, the OHD-OKE signal at long time essentially comes from the orientational relaxation of the imidazolium cation.[48]

The OHD-OKE decays as a function of water concentration are shown in black in Figure 4A and are offset along the vertical axis for clarity. Note the log axes. The data span up to six decades in time, and some decays span six decades in amplitude. The gelling region is between the OmimCl:water 1:2 and 1:4.5 samples, but it is difficult to identify this region by looking at the OHD-OKE data. At early time in the water-poor samples, a weak oscillation, known as the boson peak, appears around 2 ps.[60,61] All the decays show power law decays at early to intermediate time and at least one exponential decay at long time. As in previous OHD-OKE studies of RTIL/water mixtures,[48] most of the decays presented here are clearly biexponential at long time. Figure 4B shows a blow up of the data for the concentration ratio 1:4.5, which is on the water-rich side of the gelling region. The decay covers more than six decades in amplitude and more than five decades in time. At short time, the data are a power law, which appears as a straight line on a log plot. At longer times, the two exponential decays are manifested as "knees" in the data. As can be seen in Figure 4A, the only two decays that are single exponential are the pure OmimCl (no water added) and the most water-rich mixture (OmimCl:water = 1:100). As water is added to the pure OmimCl (and the viscosity decreases), the orientational dynamics speed up and the decay becomes biexponential, with the two exponential decay time constants becoming increasingly different up to the gelation boundary. As the water content continues to be increased after the gelling region on the high water content side, the biexponential decay time constants grow closer together. The amplitude of the slow

Figure 4. (A) OHD-OKE decays for the OmimCl/water system for various water concentrations (solid black curves) and fits to eq 9 or 10 (dashed red curves). Note the logarithmic axes. Stable gel formation occurs between the OmimCl:water = 1:2 and 1:4.5 samples. (B) A blow up of the 1:4.5 curve showing the power law region and the two exponential decays.

exponential dies away as water is added until its amplitude is so small that it is unresolvable in the OmimCl:water 1:100 sample.

Biexponential orientational decays can arise from one of two scenarios. In the first, there are two separate subensembles in the system that each has its own characteristic orientational dynamics. An example would be the core and shell waters in a reverse micelle.[62] The second scenario leading to biexponential decays is known as wobbling-in-a-cone (WC), in which a single ensemble undergoing orientational relaxation has two time scales of motion.[63,64] The fast exponential arises from diffusion over a limited range of angles, the cone, while the slow exponential decay is caused by a complete randomization of the orientation. In the absence of the final slow decay, WC would lead to a sampling of a limited set of orientations and a plateau in the anisotropy decay with no further sampling of orientations. The slow decay takes the plateau to zero orientational anisotropy. WC behavior is seen in systems in which the reorienting species is tethered to a large species, like a protein or polymer, which diffuses very slowly.[65,66] The tether restricts the range of angles that can be sampled, but on a much longer time scale, the large species undergoes orientational relaxation taking the tethered species with it. In the RTIL/water mixtures studied here and in a previous study,[48] there is no indication that there are two cation subensembles in the system. The mixtures are macroscopically homogeneous, and the volume fraction of water at which the biexponential behavior becomes apparent is small (~4%). Thus, it seems physically unrealistic that such a small amount of water can generate two distinct cation subensembles. Instead, we interpret the biexponential decays in terms of the WC model.

In the WC model, the orientational correlation function has the form[63,64,67]

$$C_2(t) = [S^2 + (1 - S^2) \exp(-t/\tau_c)] \exp(-t/\tau_m) \qquad (1)$$

where S^2 is called the order parameter, τ_c is the decay time for angular diffusion in the cone, and τ_m is the long decay time for complete orientational relaxation. The order parameter obeys the relation $0 < S^2 \leq 1$. Its functional form across a phase transition determines the order of the phase transition. For first order phase transitions, S^2 is discontinuous across the phase boundary; for second order transitions, it is continuous but its first derivative is discontinuous.[68] Because of the cone, it is not meaningful to directly compare decay times. Instead, diffusion constants must be compared, and the diffusion constant for reorientation within the cone, D_c, is given by

$$D_c = \frac{x_c^2(1 + x_c)^2\{\ln[(1 + x_c)/2] + (1 - x_c)/2\}}{\tau_c(1 - S^2)[2(x_c - 1)]}$$
$$+ \frac{(1 - x_c)(6 + 8x_c - x_c^2 - 12x_c^3 - 7x_c^4)}{24\tau_c(1 - S^2)} \qquad (2)$$

where $x_c = \cos\theta$, and θ is the cone semiangle, which is related to S^2 by

$$S^2 = \left[\frac{1}{2}\cos\theta(1 + \cos\theta)\right]^2 \qquad (3)$$

As discussed previously, we interpret the cone-limited motions as arising from the orientational dynamics of the imidazolium headgroup of the cation and the slower dynamics as the overall cation reorientation that includes the alkyl chain.[48] This assignment is supported by the fact that N-methylimidazolium is more anisotropically polarizable than octane[69,70] and that imidazolium ionic liquids give greater OHD-OKE signal than isoviscous light paraffin oils.[48] Furthermore, the assignment of the fast motions to the headgroup and the slow motions to the tail has been suggested previously for the dynamics of amphiphiles in lipid bilayers (see the Supporting Information of Busch et al.[71]). Thus, the total orientational correlation function can be broken into the correlation functions of the imidazolium headgroup, $C_h(t)$, and the entire cation including the alkyl tail, $C_c(t)$,

$$C(t) = \frac{RC_h(t) + C_c(t)}{R + 1} \qquad (4)$$

where R is the cation headgroup-to-tail OHD-OKE signal ratio and

$$C_h(t) = [S^2 + (1 - S^2) \exp(-t/\tau_c)] \exp(-t/\tau_m) \qquad (5)$$

$$C_c(t) = \exp(-t/\tau_m) \qquad (6)$$

Combining eqs 4−6 yields

$$C(t) = \frac{1}{R + 1}(R(1 - S^2) \exp[-t/\tilde{\tau}] + (RS^2 + 1)$$
$$\exp[-t/\tau_m]) \qquad (7)$$

where

$$\tilde{\tau} = (\tau_c^{-1} + \tau_m^{-1})^{-1} \qquad (8)$$

Following the previously developed procedure for estimating the cation headgroup-to-tail OHD-OKE signal ratio (R),[48] the OmimCl RTIL gave $R = 11$.

OHD-OKE data with a single long time exponential decay are often fit to a semiempirical function based on mode coupling theory (MCT) of the form

$$F(t) = [at^{-s} + pt^{-z} + dt^{b-1}]\exp(-t/\tau_m) \qquad (9)$$

Equation 9 (or a simplified one or two power law version) has been shown to fit a wide variety of systems well.[72−76] The power laws and exponential are asymptotic solutions to the MCT equations over specific time scales. The power laws are generally ascribed to caging motions, and the exponential represents the final, diffusive relaxation of the orientation. For molecules of arbitrary symmetry, P_2 orientational diffusion can give rise to up to five exponential decays,[57] but in OHD-OKE data, only one exponential decay is typically observed.[72−76] The integral of eq 9 is the sum of three incomplete gamma functions that at long-time approach $[c_1 t^{-s+1} + c_2 t^{-z+1} + c_3 t^b]\exp(-t/\tau_m)$, where c_1−c_3 are constants. Thus, the decay time, τ_m, from eq 9 (a fit to the derivative of the correlation function) is the slow part of the P_2 orientational correlation function, i.e., rotational diffusion. Because many of the OHD-OKE decays presented here display biexponential dynamics, they were fit to a function that combines eq 7 (the WC model) with the single power law version of eq 9

$$F(t) = dt^{b-1}\left(\frac{R(1-S^2)}{\tilde{\tau}}\exp[-t/\tilde{\tau}] + \frac{RS^2+1}{\tau_m}\right.$$
$$\left. \exp[-t/\tau_m]\right) \qquad (10)$$

The single power law is used because we are not interested in the very short time dynamics, but the slowest power law is necessary in the fits because it affects fitting to obtain the long time scale exponential or biexponential relaxations. Equation 10 is similar to the biexponential fitting function used previously[48] but only has one power law. It directly accounts for the derivative nature of the OHD-OKE dynamics and the signal ratio R. The $R + 1$ normalization constant from eq 7 has been subsumed into the constant d.

The use of eq 10 to find the order parameter is complicated by a number of factors and requires some comment. First, while the power law term is necessary to fit the data, it cannot be normalized at the correlation function level and makes a determination of the absolute value of S^2 impossible. Thus, the S^2 values are reported here to show trends rather than to calculate the absolute values of the order parameter and cone angle. As such, we will refer to them as the "relative" order parameter and "relative" cone angle. The second consideration is that the WC model does not account for the non-diffusive motions that give rise to power laws. By including the power law in eq 10, the "relative" order parameter, "relative" cone angle, and WC diffusion constant (D_c) describe both the diffusive and non-diffusive motions of the cone-limited cation headgroup. The overall cation relaxation, as determined by its diffusive and non-diffusive motions, is not included. This clear separation of headgroup vs overall relaxation is better than the previous approach in which all non-diffusive motions were included in the WC parameters.[48]

The pure OmimCl sample was fit with the double power law version of eq 9 beginning at 10 ps to avoid the boson peak oscillation. The most dilute sample, the OmimCl:water 1:100, was fit, starting at 1 ps, to the single power law version of eq 9. The two orientational decay times from these fits are 320 ns

and 140 ps, respectively. All other samples could not be satisfactorily fit to a single exponential function and were instead fit to eq 10. These fits begin at 1 ps. All the fits are displayed as red dashed lines in Figure 4 and are good to excellent over the entire range, with the samples closest to the gelling region showing the worst agreement. All the decay times and WC model parameters are shown in Table 1. Also shown in Table 1 are the ratios of the two orientational time scales ($6D_c\tau_m$). A larger value of ($6D_c\tau_m$) means that there is a larger difference between the fast and slow time scales. Starting on the low water content side of the gel region, this ratio increases as water is added until the system gels (OmimCl:water = 1:2). Then, on the high water content edge of the gel transition (OmimCl:water = 1:4.5), the ratio decreases as more water moves the system away from the gel region.

A simple treatment of rotational diffusion uses the Debye–Stokes–Einstein (DSE) equation

$$\tau_{self} = \frac{1}{6D_\theta} = \frac{\eta(T)Vf_\theta}{k_BT} \qquad (11)$$

where D_θ is the rotational diffusion constant, $\eta(T)$ is the temperature-dependent shear viscosity of the fluid, V is the volume of the rotating species, k_B is Boltzmann's constant, T is the absolute temperature, and f_θ is the shape-dependent friction factor, which is analytically known for a variety of shapes.[77−80] As noted in eq 11, the DSE equation is only strictly valid for self-correlations. The OHD-OKE, however, measures collective correlations. In the rotational diffusion limit, the two can be related by[81]

$$\tau_{OKE} = \tau_{collective} = \frac{g_2}{j_2}\tau_{self} \qquad (12)$$

g_2 is the static orientational correlation factor which represents the equilibrium ordering in the system, and j_2 is the dynamic orientational correlation factor which accounts for angular velocity correlations. Both factors are generally ~1.[53,81−83] Within this framework, we interpret the long-time exponential decay(s) of the OHD-OKE data as the orientational diffusion self-correlation time. Clearly, approximations are made with this assignment, but the DSE equation has been shown to fit OHD-OKE data well for a wide variety of liquids over ranges of temperatures.[72,73,84−87]

Using the fits from eqs 9 and 10, the OmimCl/water decay times are plotted in DSE fashion in Figures 5 and 6. Figure 5 shows the cone-limited decay time, τ_c, as well as the inverse diffusion constant (plotted as $1/6D_c$). The gelling region is shown in blue. DSE dynamics, as predicted using the slowest $1/6D_c$ decay time, are indicated by the dashed line. The data do follow the overall trend predicted by the DSE equation—the dynamics speed up as the overall viscosity is reduced through addition of water—but they do not show the predicted linear dependence on viscosity. Instead, the dynamics of the intermediate concentrations are faster than the DSE line. Figure 6 displays a DSE type plot for the overall cation reorientation time, τ_m. Because the large range of decay times makes it difficult to see all the data on a linear plot, the data are displayed on a logarithmic plot. Again, the gelling region is shown in blue and DSE behavior (as predicted from the maximum value of τ_m) is shown by the dashed line. Unlike the fast decay time, the slow decay is slower than the DSE prediction. As the gelling region is approached from the low water content side, the orientational relaxation changes much

Figure 5. DSE type plot for the fast imidazolium headgroup reorientational decay times. The cone-limited decay time (τ_c) is shown in black, and the inverse diffusion constant within the cone ($1/6D_c$) is shown in red. The DSE equation, as predicted using the maximum $1/6D_c$ value, is the dashed black line. The concentration range in which the stable gel forms is shown in blue.

Figure 6. DSE type plot for the slow, overall cation complete orientational randomization decay times, τ_m. The DSE equation, as predicted using the maximum τ_m value, is the dashed black line. The concentration range in which the stable gel forms is shown in blue.

slower than would be expected from the change in viscosity. On the high and low water content sides of the gelling region, there is essentially no change in the orientational relaxation, although the viscosity changes by more than a factor of 2. In the dilute region, the sample OmimCl/water = 1:30 (viscosity = ~0.05 P)

has slower orientational relaxation than the more viscous OmimCl/water = 1:15 (viscosity = ~0.2 P) sample. The error bars just barely overlap, so it is possible the slower orientational relaxation for the 1:30 sample is not real. However, the slowing for the 1:30 sample may be real and arise from the formation of micelles around the 1:30 concentration.[40]

In previous experiments on 1-alkyl-3-methylimidazolium tetrafluoroborate RTILs ($C_n$mimBF$_4$) mixed with water, the first clearly biexponential OHD-OKE decays were reported, and it was proposed that they were indicative of the approach to water-induced gelation.[48] The fast component of the biexponential decay corresponds to the motions of the imidazolium headgroup which is tethered to the alkyl tail. The slow component of the orientational dynamics is the overall cation reorientation. As water is added to the RTIL, it is localized to the ionic portion of the RTIL and, as a low viscosity liquid, allows the cationic headgroup to orientationally diffuse more quickly. Simultaneously, the hydrophobic effect causes the alkyl tails to aggregate and become locked up, thus slowing down the overall cation reorientation. Because the fast imidazolium headgroup is attached to the slow alkyl tails, its range of angular motion is limited in a cone of angles. In this picture, the water-induced slowing down of the alkyl tail reorientation eventually leads to gelation, although the $C_n$mimBF$_4$ samples phase separate before the gelation concentration can be reached.

The OmimCl/water data presented here have some similarities and differences with the previous $C_n$mimBF$_4$/water results.[48] The most apparent similarity is the clearly biexponential dynamics, which are most distinct for the long alkyl lengths of $C_n$mimBF$_4$/water at the concentration of RTIL:water ~1:3, which should be just before gelation if the $C_n$mimBF$_4$/water systems did not phase separate prior to the gel transition. Given that these are the only two sets of OHD-OKE experiments with such clearly visible biexponential decays, that the OmimCl/water system undergoes gelation, and that the $C_n$mimBF$_4$ system only differs in the type of anion, it is reasonable that the dynamics associated with the onset of gelation are responsible for such biexponential decays. A second similarity between the two RTIL/water systems is the trend in the fast component corresponding to the imidazolium headgroup motions. In both systems, as water is added, it speeds up. Because the imidazolium headgroup is the species interacting with the less viscous water, one would expect its motions to speed up as the volume fraction of water is increased.

Another similarity between the two RTIL/water systems is the reduction of the amplitude of the slow component of the OHD-OKE signal as water is added to the pure RTIL. However, because the OHD-OKE signal is the derivative of the

Table 2. OmimBF$_4$/Water Mixture DSE and Wobbling-in-a-Cone Parameters

sample (mole ratio OmimBF$_4$:water)	mole fraction water[a]	viscosity[a] (cP)	τ_c[b] (ns)	τ_m[b] (ns)	$1/6D_c$[b] (ns)	$6D_c\tau_m$	"relative" order parameter S^2[b]	"relative" cone angle θ^c (deg)
934:1 (pure)	0.00107	352		9.98				
14:1	0.0685	243		8.66				
6:1	0.148	174		6.73				
3:1	0.246	116	5.58	7.83	28.1	0.28	0.48	39
1:1	0.497	54.9	1.49	5.90	3.01	2	0.50	38
1:2.5 (satd)	0.716	24.2	0.708	6.25	1.35	5	0.55	35

[a]From ref 48, error bars ±1%. [b]Error bars: ±10%. [c]Error bars: ±5%.

correlation function, it is not necessarily the case that the orientational correlation function shows the same behavior. By fitting the OmimCl/water data to eq 10, which takes into account that the OHD-OKE signal is the derivative of the correlation function, the amplitude of the slow component at the correlation function level, (e.g., the "relative" order parameter S^2) *slightly decreases* as the gelling region is approached from the water-poor side (increase in water) and *significantly increases* as the gelling region is approached from the water-rich side (decrease in water). In the previous $C_n$mimBF$_4$/water studies, the order parameter becomes slightly larger as the gelation point is approached from the pure RTIL side (increase in water). However, those order parameters had large error bars and were extracted using a different fitting function which accounted for all non-diffusive motions in the order parameter (including non-diffusive overall cation reorientation). Thus, to compare the two data sets, the biexponential OmimBF$_4$/water data from the earlier study[48] were refit with eq 10 and the results are reported in Table 2 along with the decay parameters for the single exponential OmimBF$_4$/water data. With the newer fitting approach, the OmimBF$_4$/water "relative" order parameter *slightly increases* as gelling concentration is approached when water is added to the pure RTIL. This is the opposite trend seen in the OmimCl/water system in this concentration regime and suggests that the order of the phase transitions between the two RTIL/water systems may be different.

The other difference between the OmimCl/water and $C_n$mimBF$_4$/water data sets is the trend in the slow component of the orientational dynamics. In the long-chain $C_n$mimBF$_4$ samples (octyl and decyl), the slow component stops getting faster as the viscosity decreases through addition of water. For the decyl side chain (DmimBF$_4$), the decay time actually gets longer as water is added and the viscosity is reduced (anti-DSE behavior). The slowdown of the overall cation orientational relaxation was interpreted as resulting from water interactions with the ions inducing a structural organization of the alkyl chains that locks them up and inhibits reorientation. It was suggested that this behavior might be a precursor to the onset of water-induced gelation but that the mixture phase separates before gelation can occur. However, in the OmimCl/water data presented here, the trend in the slow dynamics is to get faster as water is added and the gel point is approached from the water-poor side. This difference in the two systems does not necessarily mean that the interpretation of the slow component of the dynamics is incorrect. First, the overall cation relaxation time (τ_m) for intermediate concentrations of the OmimCl/water system is always slower than the DSE prediction (see Figure 6). Alkyl tail aggregation and the onset of gelation is still a reasonable interpretation for such behavior. Second, at the boundaries of the gelling region, the overall Omim cation reorientational dynamics are the same (see Figure 6), which again is consistent with the gelation proposal. One might expect that if the approach to gelation causes the alkyl tails to aggregate, slowing down the cation reorientation, there would be concentrations on either side of the gelation region at which the cation reorientation times would be identical. Third, the ratio of the slow component to the fast component for both RTIL/water systems ($6D_c\tau_m$, reported in Tables 1 and 2) peaks near the gelling region. Even without the previous $C_n$mimBF$_4$/water data for comparison, the gelation onset hypothesis still would have been invoked to explain these three observations in the OmimCl/water data.

The question then becomes why does the overall cation reorientation in the $C_n$mimBF$_4$/water system slow down dramatically as water is added, while the OmimCl/water system does not show this behavior? Instead, the overall cation reorientation in the OmimCl/water system monotonically speeds up as water is added and the gelation point is approached from the water-poor side. We propose that the answer may lie in the nature of the liquid/gel phase transitions. In thermotropic nematic liquid crystals, the temperature-dependent isotropic–nematic phase transition is continuous and weakly first order. The orientational dynamics follow a modified form of the DSE equation developed by de Gennes[88]

$$\tau_{\text{self}} = \frac{1}{6D_\theta} = \frac{\eta(T)Vf_\theta}{k_B(T - T^*)^\gamma} \tag{13}$$

Here T^* is the critical temperature which is usually a degree below the isotropic-to-nematic phase transition temperature, and γ is called the critical exponent. In thermotropic liquid crystals, $\gamma \approx 1$.[89] Lyotropic liquid crystals, such as the OmimCl/water system, display first order phase transitions that are *both* concentration- and temperature-dependent. This gives rise to dynamics of the form[90]

$$\tau_{\text{self}} \propto \frac{\eta(T, X_w)}{[T - T^* + a(X_w^* - X_w)]^\gamma} \tag{14}$$

where X_w is the mole fraction of one component of the system (in this case, water), X_w^* is the critical concentration near the phase transition concentration, and a is a proportionality constant. The concentration dependence of the phase transition of lyotropic liquid crystals is much less studied than the temperature dependence, and the parameters X_w^* and a are generally harder to measure and thus not as well-known. Furthermore, it has been shown that the concentration can influence the nature of the temperature-dependent phase transition, even changing it from first to second order,[90] and that the amphiphile counterion can modulate transition temperatures and concentrations.[91] Thus, there is no reason to require that the trend in overall cation reorientational dynamics between two RTIL/water systems with different anions be the same. For example, in switching from OmimCl to OmimBF$_4$, it is possible for the change of anion to shift the transition concentration to a regime in which the transition changes from first to second order. In turn, this can influence the trend in the dynamics, from the rather discontinuous jump in τ_m at the water-poor gelation boundary in OmimCl/water to the more continuous slowdown seen in the $C_n$mimBF$_4$/water data. Thus, we suggest that the difference between the OmimCl/water and $C_n$mimBF$_4$/water systems in both the DSE behavior for the slow component of the dynamics and the trend in "relative" order parameter may indicate that the type of concentration-dependent phase transition (first order, weakly first order, or second order) may be tuned by the choice of the RTIL anion.

IV. CONCLUDING REMARKS

Optical heterodyne-detected optical Kerr effect experiments on the room temperature ionic liquid 1-methyl-3-octylimidazolium chloride mixed with water have been presented. This binary mixture forms a stable gel between the water mole fractions 0.69 and 0.81, and is, to the best of our knowledge, the smallest molecular weight gel known. The optical Kerr effect decays for intermediate water concentrations are distinctly biexponential,

similar to the previous experiments on 1-alkyl-3-methylimidazolium tetrafluoroborate/water mixtures.[48]

We analyze the biexponential decays with the wobbling-in-a-cone model in which the fast, cone-limited motions correspond to the imidazolium headgroup restricted reorientation and the slow motions to the complete orientational relaxation of the liquid that occurs with the entire cation, headgroup plus alkyl chain. The extracted "relative" order parameters indicate that, as the OmimCl/water gelling concentration is approached from the water-poor side, the motions of the imidazolium headgroup become less restricted. In contrast, as the gelling region is approached from the water-rich side, the headgroup motions become more restricted. Reanalysis of some of the previous $C_n$mimBF$_4$/water data[48] indicates that as water is added to the pure RTIL the headgroup motions become more restricted. The overall cation reorientation time in the OmimCl/water samples is anomalously slow compared to the DSE equation calculation, with the samples near the gelation boundaries showing no change in decay time despite a difference in viscosity. We have proposed that the biexponential decays are a precursor to the onset of gelation. Furthermore, the difference in the trends of the overall cation reorientation and the "relative" order parameter between RTIL/water systems with different anions suggests that the order of the phase transition can be tuned by the choice of anion.

■ AUTHOR INFORMATION

Corresponding Author
*E-mail: fayer@stanford.edu. Phone: 650 723-4446.

Notes
The authors declare no competing financial interest.

■ REFERENCES

(1) Plechkova, N. V.; Seddon, K. R. Applications of Ionic Liquids in the Chemical Industry. *Chem. Soc. Rev.* **2008**, *37*, 123–150.
(2) Hallett, J. P.; Welton, T. Room-Temperature Ionic Liquids: Solvents for Synthesis and Catalysis. 2. *Chem. Rev.* **2011**, *111*, 3508–3576.
(3) Lewandowski, A.; Swiderska-Mocek, A. Ionic Liquids as Electrolytes for Li-Ion Batteries-an Overview of Electrochemical Studies. *J. Power Sources* **2009**, *194*, 601–609.
(4) Reichert, W. M.; Holbrey, J. D.; Vigour, K. B.; Morgan, T. D.; Broker, G. A.; Rogers, R. D. Approaches to Crystallization from Ionic Liquids: Complex Solvents-Complex Results, or, a Strategy for Controlled Formation of New Supramolecular Architectures? *Chem. Commun.* **2006**, 4767–4779.
(5) Dobler, D.; Schmidts, T.; Klingenhofer, I.; Runkel, F. Ionic Liquids as Ingredients in Topical Drug Delivery Systems. *Int. J. Pharm.* **2013**, *441*, 620–627.
(6) Hu, X. D.; Zhang, S. G.; Liu, Y.; Qu, C.; Lu, L. J.; Ma, X. Y.; Zhang, X. P.; Deng, Y. Q. Electrowetting Based Infrared Lens Using Ionic Liquids. *Appl. Phys. Lett.* **2011**, *99*, 213505.
(7) Armand, M.; Endres, F.; MacFarlane, D. R.; Ohno, H.; Scrosati, B. Ionic-Liquid Materials for the Electrochemical Challenges of the Future. *Nat. Mater.* **2009**, *8*, 621–629.
(8) Hagfeldt, A.; Boschloo, G.; Sun, L. C.; Kloo, L.; Pettersson, H. Dye-Sensitized Solar Cells. *Chem. Rev.* **2010**, *110*, 6595–6663.
(9) Taylor, A. W.; Qiu, F. L.; Hu, J. P.; Licence, P.; Walsh, D. A. Heterogeneous Electron Transfer Kinetics at the Ionic Liquid/Metal Interface Studied Using Cyclic Voltammetry and Scanning Electrochemical Microscopy. *J. Phys. Chem. B* **2008**, *112*, 13292–13299.
(10) Yung, K. Y.; Schadock-Hewitt, A. J.; Hunter, N. P.; Bright, F. V.; Baker, G. A. 'Liquid Litmus': Chemosensory Ph-Responsive Photonic Ionic Liquids. *Chem. Commun.* **2011**, *47*, 4775–4777.
(11) Brown, P.; Butts, C. P.; Eastoe, J.; Hernandez, E. P.; Machado, F. L. D.; de Oliveira, R. J. Dication Magnetic Ionic Liquids with Tuneable Heteroanions. *Chem. Commun.* **2013**, *49*, 2765–2767.
(12) Holbrey, J. D.; Seddon, K. R. The Phase Behaviour of 1-Alkyl-3-Methylimidazolium Tetrafluoroborates; Ionic Liquids and Ionic Liquid Crystals. *J. Chem. Soc., Dalton Trans.* **1999**, 2133–2139.
(13) Ji, Y. M.; Shi, R.; Wang, Y. T.; Saielli, G. Effect of the Chain Length on the Structure of Ionic Liquids: From Spatial Heterogeneity to Ionic Liquid Crystals. *J. Phys. Chem. B* **2013**, *117*, 1104–1109.
(14) Triolo, A.; Russina, O.; Bleif, H. J.; Di Cola, E. Nanoscale Segregation in Room Temperature Ionic Liquids. *J. Phys. Chem. B* **2007**, *111*, 4641–4644.
(15) Hardacre, C.; Holbrey, J. D.; Mullan, C. L.; Youngs, T. G. A.; Bowron, D. T. Small Angle Neutron Scattering from 1-Alkyl-3-Methylimidazolium Hexafluorophosphate Ionic Liquids ([C(N)Mim]-[PF6], N=4, 6, and 8). *J. Chem. Phys.* **2010**, *133*, 074510.
(16) Annapureddy, H. V. R.; Kashyap, H. K.; De Biase, P. M.; Margulis, C. J. What Is the Origin of the Prepeak in the X-Ray Scattering of Imidazolium-Based Room-Temperature Ionic Liquids? *J. Phys. Chem. B* **2010**, *114*, 16838–16846.
(17) Kagimoto, J.; Nakamura, N.; Kato, T.; Ohno, H. Novel Thermotropic Gels Composed of Only Ions. *Chem. Commun.* **2009**, 2405–2407.
(18) Le Bideau, J.; Viau, L.; Vioux, A. Ionogels, Ionic Liquid Based Hybrid Materials. *Chem. Soc. Rev.* **2011**, *40*, 907–925.
(19) Hanabusa, K.; Fukui, H.; Suzuki, M.; Shirai, H. Specialist Gelator for Ionic Liquids. *Langmuir* **2005**, *21*, 10383–10390.
(20) Firestone, M. A.; Dzielawa, J. A.; Zapol, P.; Curtiss, L. A.; Seifert, S.; Dietz, M. L. Lyotropic Liquid-Crystalline Gel Formation in a Room-Temperature Ionic Liquid. *Langmuir* **2002**, *18*, 7258–7260.
(21) Firestone, M. A.; Rickert, P. G.; Seifert, S.; Dietz, M. L. Anion Effects on Ionogel Formation in N,N ′-Dialkylimidazolium-Based Ionic Liquids. *Inorg. Chim. Acta* **2004**, *357*, 3991–3998.
(22) Goodchild, I.; Collier, L.; Millar, S. L.; Prokes, I.; Lord, J. C. D.; Butts, C. P.; Bowers, J.; Webster, J. R. P.; Heenan, R. K. Structural Studies of the Phase, Aggregation and Surface Behaviour of 1-Alkyl-3-Methylimidazolium Halide Plus Water Mixtures. *J. Colloid Interface Sci.* **2007**, *307*, 455–468.
(23) Ribot, J. C.; Guerrero-Sanchez, C.; Hoogenboom, R.; Schubert, U. S. Aqueous Gelation of Ionic Liquids: Reverse Thermoresponsive Ion Gels. *Chem. Commun.* **2010**, *46*, 6971–6973.
(24) Bhargava, B. L.; Klein, M. L. Formation of Micelles in Aqueous Solutions of a Room Temperature Ionic Liquid: A Study Using Coarse Grained Molecular Dynamics. *Mol. Phys.* **2009**, *107*, 393–401.
(25) Ries, L. A. S.; do Amaral, F. A.; Matos, K.; Martini, E. M. A.; de Souza, M. O.; de Souza, R. F. Evidence of Change in the Molecular Organization of 1-N-Butyl-3-Methylimidazolium Tetrafluoroborate Ionic Liquid Solutions with the Addition of Water. *Polyhedron* **2008**, *27*, 3287–3293.
(26) Dorbritz, S.; Ruth, W.; Kragl, U. Investigation on Aggregate Formation of Ionic Liquids. *Adv. Synth. Catal.* **2005**, *347*, 1273–1279.
(27) Almasy, L.; Turmine, M.; Perera, A. Structure of Aqueous Solutions of Ionic Liquid 1-Butyl-3-Methylimidazolium Tetrafluoroborate by Small-Angle Neutron Scattering. *J. Phys. Chem. B* **2008**, *112*, 2382–2387.
(28) Vanyur, R.; Biczok, L.; Miskolczy, Z. Micelle Formation of 1-Alkyl-3-Methylimidazolium Bromide Ionic Liquids in Aqueous Solution. *Colloids Surf., A* **2007**, *299*, 256–261.
(29) Rilo, E.; Vila, J.; Pico, J.; Garcia-Garabal, S.; Segade, L.; Varela, L. M.; Cabeza, O. Electrical Conductivity and Viscosity of Aqueous

Binary Mixtures of 1-Alkyl-3-Methyl Imidazolium Tetrafluoroborate at Four Temperatures. *J. Chem. Eng. Data* **2010**, *55*, 639−644.

(30) Takamuku, T.; Kyoshoin, Y.; Shimomura, T.; Kittaka, S.; Yamaguchi, T. Effect of Water on Structure of Hydrophilic Imidazolium-Based Ionic Liquid. *J. Phys. Chem. B* **2009**, *113*, 10817−10824.

(31) Masaki, T.; Nishikawa, K.; Shirota, H. Microscopic Study of Ionic Liquid-H₂O Systems: Alkyl-Group Dependence of 1-Alkyl-3-Methylimidazolium Cation. *J. Phys. Chem. B* **2010**, *114*, 6323−6331.

(32) Danten, Y.; Cabaco, M. I.; Besnard, M. Interaction of Water Highly Diluted in 1-Alkyl-3-Methyl Imidazolium Ionic Liquids with the PF_6^- and BF_4^- Anions. *J. Phys. Chem. A* **2009**, *113*, 2873−2889.

(33) Luczak, J.; Hupka, J.; Thoming, J.; Jungnickel, C. Self-Organization of Imidazolium Ionic Liquids in Aqueous Solution. *Colloids Surf., A* **2008**, *329*, 125−133.

(34) Chang, H. C.; Jiang, J. C.; Liou, Y. C.; Hung, C. H.; Lai, T. Y.; Lin, S. H. Effects of Water and Methanol on the Molecular Organization of 1-Butyl-3-Methylimidazolium Tetrafluoroborate as Functions of Pressure and Concentration. *J. Chem. Phys.* **2008**, *129*, 044506.

(35) Miskolczy, Z.; Sebok-Nagy, K.; Biczok, L.; Gokturk, S. Aggregation and Micelle Formation of Ionic Liquids in Aqueous Solution. *Chem. Phys. Lett.* **2004**, *400*, 296−300.

(36) Fazio, B.; Triolo, A.; Di Marco, G. Local Organization of Water and Its Effect on the Structural Heterogeneities in Room-Temperature Ionic Liquid/H₂O Mixtures. *J. Raman Spectrosc.* **2008**, *39*, 233−237.

(37) Shirota, H.; Biswas, R. Intermolecular/Interionic Vibrations of 1-Methyl-3-N-Octylimidazolium Tetrafluoroborate Ionic Liquid and H2o Mixtures. *J. Phys. Chem. B* **2012**, *116*, 13765−13773.

(38) Smirnova, N. A.; Safonova, E. A. Micellization in Solutions of Ionic Liquids. *Colloid J.* **2012**, *74*, 254−265.

(39) Schroder, C.; Rudas, T.; Neumayr, G.; Benkner, S.; Steinhauser, O. On the Collective Network of Ionic Liquid/Water Mixtures. I. Orientational Structure. *J. Chem. Phys.* **2007**, *127*, 234503.

(40) Bowers, J.; Butts, C. P.; Martin, P. J.; Vergara-Gutierrez, M. C.; Heenan, R. K. Aggregation Behavior of Aqueous Solutions of Ionic Liquids. *Langmuir* **2004**, *20*, 2191−2198.

(41) Ribot, J. C.; Guerrero-Sanchez, C.; Hoogenboom, R.; Schubert, U. S. Thermoreversible Ionogels with Tunable Properties Via Aqueous Gelation of an Amphiphilic Quaternary Ammonium Oligoether-Based Ionic Liquid. *J. Mater. Chem.* **2010**, *20*, 8279−8284.

(42) Inoue, T.; Dong, B.; Zheng, L. Q. Phase Behavior of Binary Mixture of 1-Dodecyl-3-Methylimidazolium Bromide and Water Revealed by Differential Scanning Calorimetry and Polarized Optical Microscopy. *J. Colloid Interface Sci.* **2007**, *307*, 578−581.

(43) Jiang, W.; Wang, Y. T.; Voth, G. A. Molecular Dynamics Simulation of Nanostructural Organization in Ionic Liquid/Water Mixtures. *J. Phys. Chem. B* **2007**, *111*, 4812−4818.

(44) Zhang, G. D.; Chen, X.; Zhao, Y. R.; Xie, Y. Z.; Qiu, H. Y. Effects of Alcohols and Counterions on the Phase Behavior of 1-Octyl-3-Methylimidazolium Chloride Aqueous Solution. *J. Phys. Chem. B* **2007**, *111*, 11708−11713.

(45) Mendez-Morales, T.; Carrete, J.; Cabeza, O.; Gallego, L. J.; Varela, L. M. Molecular Dynamics Simulation of the Structure and Dynamics of Water-1-Alkyl-3-Methylimidazolium Ionic Liquid Mixtures. *J. Phys. Chem. B* **2011**, *115*, 6995−7008.

(46) Balevicius, V.; Gdaniec, Z.; Aidas, K.; Tamuliene, J. NMR and Quantum Chemistry Study of Mesoscopic Effects in Ionic Liquids. *J. Phys. Chem. A* **2010**, *114*, 5365−5371.

(47) Spohr, H. V.; Patey, G. N. The Influence of Water on the Structural and Transport Properties of Model Ionic Liquids. *J. Chem. Phys.* **2010**, *132*.

(48) Sturlaugson, A. L.; Fruchey, K. S.; Fayer, M. D. Orientational Dynamics of Room Temperature Ionic Liquid/Water Mixtures: Water-Induced Structure. *J. Phys. Chem. B* **2012**, *116*, 1777−1787.

(49) Gomez, E.; Gonzalez, B.; Dominguez, A.; Tojo, E.; Tojo, J. Dynamic Viscosities of a Series of 1-Alkyl-3-Methylimidazolium Chloride Ionic Liquids and Their Binary Mixtures with Water at Several Temperatures. *J. Chem. Eng. Data* **2006**, *51*, 696−701.

(50) Smith, N. A.; Meech, S. R. Optically-Heterodyne-Detected Optical Kerr Effect (OHD-OKE): Applications in Condensed Phase Dynamics. *Int. Rev. Phys. Chem.* **2002**, *21*, 75−100.

(51) Kinoshita, S.; Sakai, Y.; Miyazaki, J.; Watanabe, J. Fundamental Aspects of Light Scattering and Optical Kerr Effect Spectroscopy. *Eur. Phys. J.: Spec. Top.* **2012**, *209*, 1−100.

(52) Annapureddy, H. V. R.; Hu, Z. H.; Xia, J. C.; Margulis, C. J. How Does Water Affect the Dynamics of the Room-Temperature Ionic Liquid 1-Hexyl-3-Methylimidazolium Hexafluorophosphate and the Fluorescence Spectroscopy of Coumarin-153 When Dissolved in It? *J. Phys. Chem. B* **2008**, *112*, 1770−1776.

(53) Deeg, F. W.; Stankus, J. J.; Greenfield, S. R.; Newell, V. J.; Fayer, M. D. Anisotropic Reorientational Relaxation of Biphenyl - Transient Grating Optical Kerr Effect Measurements. *J. Chem. Phys.* **1989**, *90*, 6893−6902.

(54) Ruhman, S.; Williams, L. R.; Joly, A. G.; Kohler, B.; Nelson, K. A. Nonrelaxational Inertial Motion in Cs2 Liquid Observed by Femtosecond Time-Resolved Impulsive Stimulated Scattering. *J. Phys. Chem.* **1987**, *91*, 2237−2240.

(55) Yan, Y. X.; Nelson, K. A. Impulsive Stimulated Light-Scattering 0.1. General-Theory. *J. Chem. Phys.* **1987**, *87*, 6240−6256.

(56) Palese, S.; Schilling, L.; Miller, R. J. D.; Staver, P. R.; Lotshaw, W. T. Femtosecond Optical Kerr-Effect Studies of Water. *J. Phys. Chem.* **1994**, *98*, 6308−6316.

(57) Berne, B. J.; Pecora, R. *Dynamic Light Scattering*; J. Wiley: New York, 1976.

(58) Elola, M. D.; Ladanyi, B. M. Polarizability Response in Polar Solvents: Molecular-Dynamics Simulations of Acetonitrile and Chloroform. *J. Chem. Phys.* **2005**, *122*, 224506.

(59) Elola, M. D.; Ladanyi, B. M. Molecular Dynamics Study of Polarizability Anisotropy Relaxation in Aromatic Liquids and Its Connection with Local Structure. *J. Phys. Chem. B* **2006**, *110*, 15525−15541.

(60) Cang, H.; Li, J.; Andersen, H. C.; Fayer, M. D. Boson Peak in Supercooled Liquids: Time Domain Observations and Mode Coupling Theory. *J. Chem. Phys.* **2005**, *123*, 64508−64508.

(61) Li, J.; Wang, I.; Fruchey, K.; Fayer, M. D. Dynamics in Supercooled Ionic Organic Liquids and Mode Coupling Theory Analysis. *J. Phys. Chem. A* **2006**, *110*, 10384−10391.

(62) Moilanen, D. E.; Fenn, E. E.; Wong, D.; Fayer, M. D. Water Dynamics in Large and Small Reverse Micelles: From Two Ensembles to Collective Behavior. *J. Chem. Phys.* **2009**, *131*, 014704.

(63) Lipari, G.; Szabo, A. Effect of Librational Motion on Fluorescence Depolarization and Nuclear Magnetic-Resonance Relaxation in Macromolecules and Membranes. *Biophys. J.* **1980**, *30*, 489−506.

(64) Wang, C. C.; Pecora, R. Time-Correlation Functions for Restricted Rotational Diffusion. *J. Chem. Phys.* **1980**, *72*, 5333−5340.

(65) Sahu, K.; Mondal, S. K.; Ghosh, S.; Roy, D.; Bhattacharyya, K. Temperature Dependence of Solvation Dynamics and Anisotropy Decay in a Protein: Ans in Bovine Serum Albumin. *J. Chem. Phys.* **2006**, *124*, 124909.

(66) Leezenberg, P. B.; Marcus, A. H.; Frank, C. W.; Fayer, M. D. Rotational Dynamics of Naphthalene-Labeled Cross-Link Junctions in Poly(Dimethylsiloxane) Elastomers. *J. Phys. Chem.* **1996**, *100*, 7646−7655.

(67) Tan, H.-S.; Piletic, I. R.; Fayer, M. D. Orientational Dynamics of Nanoscopic Water in Reverse Micelles: Ultrafast Infrared Frequency Selective Transient Absorption Experiments. *J. Chem. Phys.* **2005**, *122*, 174501(174509).

(68) Popa-Nita, V. *Phase Transitions: Applications to Liquid Crystals, Organic Electronic and Optoelectronic Fields*; Research Signpost: Kerala, India, 2006.

(69) Calder, K. E.; Calvert, R. L.; Lukins, P. B.; Ritchie, G. L. D. Magnetic Anisotropies and Relative Aromaticities of Pyrrole, Pyrazole, Imidazole and Their N-Methyl Derivatives. *Aust. J. Chem.* **1981**, *34*, 1835−1835.

(70) Shuvaeva, O. V. Calculation of the Anisotropy of Molecular Polarizability of Liquid N-Alkanes and N-Alcohols. *Russ. J. Phys. Chem. A* **2007**, *81*, 798−801.

(71) Busch, S.; Smuda, C.; Pardo, L. C.; Unruh, T. Molecular Mechanism of Long-Range Diffusion in Phospholipid Membranes Studied by Quasielastic Neutron Scattering. *J. Am. Chem. Soc.* **2010**, *132*, 3232−3233.

(72) Sturlaugson, A. L.; Fruchey, K. S.; Lynch, S. R.; Aragon, S. R.; Fayer, M. D. Orientational and Translational Dynamics of Polyether/Water Solutions. *J. Phys. Chem. B* **2010**, *114*, 5350−5358.

(73) Cang, H.; Li, J.; Fayer, M. D. Orientational Dynamics of the Ionic Organic Liquid 1-Ethyl-3-Methylimidazolium Nitrate. *J. Chem. Phys.* **2003**, *119*, 13017−13023.

(74) Cang, H.; Li, J.; Novikov, V. N.; Fayer, M. D. Dynamics in Supercooled Liquids and in the Isotropic Phase of Liquid Crystals: A Comparison. *J. Chem. Phys.* **2003**, *118*, 9303−9311.

(75) Cang, H.; Novikov, V. N.; Fayer, M. D. Logarithmic Decay of the Orientational Correlation Function in Supercooled Liquids on the Ps to Ns Time Scale. *J. Chem. Phys.* **2003**, *118*, 2800−2807.

(76) Nicolau, B. G.; Sturlaugson, A.; Fruchey, K.; Ribeiro, M. C. C.; Fayer, M. D. Room Temperature Ionic Liquid-Lithium Salt Mixtures: Optical Kerr Effect Dynamical Measurements. *J. Phys. Chem. B* **2010**, *114*, 8350−8356.

(77) Allison, S. A. Low Reynolds Number Transport Properties of Axisymmetric Particles Employing Stick and Slip Boundary Conditions. *Macromolecules* **1999**, *32*, 5304−5312.

(78) Hu, C. M.; Zwanzig, R. Rotational Friction Coefficients for Spheroids with Slipping Boundary-Condition. *J. Chem. Phys.* **1974**, *60*, 4354−4357.

(79) Perrin, F. The Brownien Movement of an Ellipsoide. - the Dielectric Dispersion of Ellipsoidal Molecules. *J. Phys. Radium* **1934**, *5*, 497−511.

(80) Tirado, M. M.; Garciadelatorre, J. Rotational-Dynamics of Rigid, Symmetric Top Macromolecules - Application to Circular-Cylinders. *J. Chem. Phys.* **1980**, *73*, 1986−1993.

(81) Madden, P. A.; Battaglia, M. R.; Cox, T. I.; Pierens, R. K.; Champion, J. The Orientational Correlation Parameter G2 of Symmetrical Benzene-Derivatives. *Chem. Phys. Lett.* **1980**, *76*, 604−608.

(82) Elola, M. D.; Ladanyi, B. M.; Scodinu, A.; Loughnane, B. J.; Fourkas, J. T. Effects of Molecular Association on Polarizability Relaxation in Liquid Mixtures of Benzene and Hexafluorobenzene. *J. Phys. Chem. B* **2005**, *109*, 24085−24099.

(83) Battaglia, M. R.; Cox, T. I.; Madden, P. A. Orientational Correlation Parameter for Liquid Cs2, C6h6 and C6f6. *Mol. Phys.* **1979**, *37*, 1413−1427.

(84) Alms, G. R.; Bauer, D. R.; Brauman, J. I.; Pecora, R. Depolarized Rayleigh-Scattering and Orientational Relaxation of Molecules in Solution 0.2. Chloroform and Nitrobenzene. *J. Chem. Phys.* **1973**, *59*, 5310−5320.

(85) Alms, G. R.; Bauer, D. R.; Brauman, J. I.; Pecora, R. Depolarized Rayleigh-Scattering and Orientational Relaxation of Molecules in Solution 0.1. Benzene, Toluene, and Para-Xylene. *J. Chem. Phys.* **1973**, *58*, 5570−5578.

(86) Bauer, D. R.; Alms, G. R.; Brauman, J. I.; Pecora, R. Depolarized Rayleigh-Scattering and C-13 Nmr-Studies of Anisotropic Molecular-Reorientation of Aromatic-Compounds in Solution. *J. Chem. Phys.* **1974**, *61*, 2255−2261.

(87) Sturlaugson, A. L.; Fayer, M. D. Temperature and Hydration-Dependent Rotational and Translational Dynamics of a Polyether Oligomer. *J. Phys. Chem. B* **2011**, *115*, 945−950.

(88) de Gennes, P. G. *The Physics of Liquid Crystals*; Clarendon: Oxford, U.K., 1974.

(89) Stankus, J. J.; Torre, R.; Marshall, C. D.; Greenfield, S. R.; Sengupta, A.; Tokmakoff, A.; Fayer, M. D. Nanosecond Time Scale Dynamics of Pseudo-Nematic Domains in the Isotropic Phase of Liquid Crystals. *Chem. Phys. Lett.* **1992**, *194*, 213−216.

(90) Puica, M.-R. Lyotropic Liquid Crystals at Phase Transitions. *Rom. Rep. Phys.* **2006**, *54*, 491−518.

(91) Sorenson, G. P.; Coppage, K. L.; Mahanthappa, M. K. Unusually Stable Aqueous Lyotropic Gyroid Phases from Gemini Dicarboxylate Surfactants. *J. Am. Chem. Soc.* **2011**, *133*, 14928−14931.